Journal of Materials Chemistry A

ARTICLE

High-Pressure Zinc Oxide Phase as Visible-Light-Active Photocatalyst with Narrow Band Gap

Received 00th January 20xx,
Accepted 00th January 20xx

DOI: 10.1039/x0xx00000x

www.rsc.org/

Hadi Razavi-Khosroshahi,[a,*] Kaveh Edalati,[b,c] Ji Wu,[b] Yuki Nakashima,[a] Makoto Arita,[c] Yoshifumi Ikoma,[c] Masaaki Sadakiyo,[b] Yuji Inagaki,[d] Aleksandar Staykov,[b] Miho Yamauchi,[b,e] Zenji Horita[b,c] and Masayoshi Fuji[a]

Wide band gap of pure ZnO with wurtzite crystal structure (3.1-3.4 eV) limits its photocatalytic activity to the ultraviolet (UV) region of solar spectrum. High-pressure rocksalt polymorph of ZnO can theoretically show narrow band gap, however the rocksalt phase is unstable at ambient pressure. In this study, rocksalt phase with large fractions of oxygen vacancies is sucessfully stabilized at ambient condition by inducing plastic strain to pure ZnO under 6 GPa using the high-pressure torsion (HPT) method. Formation of rocksalt phase reduced the band gap of ZnO to 1.8 eV, in good agreement with the first-principles calculations, and significantly improved the photocatalytic activity under visible light.

Introduction

Clean energy production[1] and degradation of organic pollutants in air/water[2, 3] by means of semiconductor photocatalysts have been in the front line of fundamental studies and technological approaches in recent decades. Zinc oxide (ZnO) with a wurtzite crystal structure is a stable, non-toxic and inexpensive semiconductor with superior photocatalytic properties[4], which is widely used as antibacterials,[5] biochemical sensors[6] and photovoltaic cells.[7] However, the photocatalytic application of pure ZnO has been limited to the UV spectrum of sunlight due to its wide band gap, 3.1-3.4 eV.[4, 8] Since UV light only accounts for ~5% of solar spectrum, there is a great interest in designing ZnO semiconductor with capability of absorbing visible light, which its fraction is ~50% of solar spectrum.[9]

To enhance solar energy absorption, an efficient photocatalyst should have a band gap in the range of 1.8-2.2 eV.[10] Although forming heterojunctions by coupling different types of semiconductors,[11, 12] modification with carbon nanotubes[13] and fullerenes,[14] and introduction of oxygen vacancies[15, 16] recently receive appreciable attention in terms of reducing the band gap, doping with cation/anion[2, 17-19] is still the main approach for the band gap narrowing of ZnO. Despite its effectiveness on controlling the band gap, doping does not necessarily result in photocatalytic activity of ZnO under visible light due to several reasons[20]: (i) precipitation of dopants can strongly change the chemical composition and activity of ZnO; (ii) the solubility of dopants in ZnO are usually very low, whereas heavy doping is required in most photocatalytic cases; (iii) ZnO is usually sintered at elevated temperatures to attain a good crystallinity, but an undesired expulsion of substituted dopant occurs when the temperature is raised; and (iv) dopants usually leach from their ZnO host at extreme pH conditions which can lead to toxicity in the solution.

Narrowing the band gap of pure semiconductors by dopant-free approaches is currently in the spotlight[21-23]. Theoretical studies on ZnO[24-26] suggested that the band gap of high-pressure rocksalt phase with the cubic crystal structure is in the range of 1.2-2.6 eV which is lower than that of the wurtzite phase with the hexagonal crystal structure. *In-situ* band gap measurements under high pressure also confirmed that the band gap of rocksalt phase is lower than that of the wurtzite phase.[24, 27, 28] However, it is evident from the phase diagram of ZnO[29] as shown in Fig. 1a, that the only stable phase of ZnO at the ambient condition is wurtzite and the rocksalt phase is only stable at pressures higher than 6-10 GPa.

High-pressure torsion (HPT) method,[30, 31] as schematically shown in Fig. 1b, is an advantageous technique for fast production of high-pressure phases. In the HPT method, sample is sandwiched between two anvils under high pressure, and severe plastic strain is induced to the sample by rotating the lower anvil with respect to the upper anvil. Introduction of large plastic strain under high pressure and resultant nanostructural changes alter the thermodynamic stability of phases not only under high pressures but also at ambient condition.[30-35] Previous studies using the HPT method showed that several nanostructured high-pressure phases could be stabilized at ambient pressure such as ω phase in Zr and

[a] *Advanced Ceramics Research Center, Nagoya Institute of Technology, Gifu, Japan.*
[b] *International Institute for Carbon-Neutral Energy Research (WPI-I2CNER), Kyushu University, Fukuoka, Japan.*
[c] *Department of Materials Science and Engineering, Faculty of Engineering, Kyushu University, Fukuoka, Japan.*
[d] *Department of Applied Quantum Physics and Nuclear Engineering, Faculty of Engineering, Kyushu University, Fukuoka, Japan.*
[e] *Department of Applied Chemistry, Faculty of Engineering, Kyushu University, Fukuoka, Japan.*
† Footnotes relating to the title and/or authors should appear here.
Electronic Supplementary Information (ESI) available: [details of any supplementary information available should be included here]. See DOI: 10.1039/x0xx00000x

Ti,[33] diamond-like phase in C,[36] cubic phase in $BaTiO_3$,[34] monoclinic phase in Y_2O_3,[37] and columbite phase with enhanced potocatalytic performance in TiO_2.[38]

In this study, a nanostructured high-pressure rocksalt ZnO phase with large fraction of oxygen vacancies is successfully stabilized by HPT method at ambient pressure, and its photocatalytic activity is examined for the first time. Both experimental results and first-principles calculations show that the band gap is considerably reduced resulting in enhanced photocatalytic activity under visible light.

Experimental and Calculation Methods

Wurtzite ZnO powder with an average particle size of ~20 nm and a purity level of 99.8 % was processed by HPT at room temperature. Plastic strain was introduced under 3 and 6 GPa by rotating the lower anvil against the upper anvil for N = 3 turns and discs with 10 mm diameter and 0.8 mm thickness were obtained (see Supplementary Information 1.1 for details). Phase transformations were examined by X-ray diffraction (XRD) analysis using the CuKα and 24.772-keV synchrotron radiations, and the fraction of each phase was estimated by Rietveld analysis. The microstructure of different phases was examined by transmission electron microscopy (TEM), and the formation of oxygen vacancies was evaluated by examining the colour of samples, Raman spectroscopy equipped with a 532 nm laser, photoluminescence (PL) spectroscopy with excitation wavelength of 488 nm, and electron paramagnetic resonance (EPR) with 10 GHz microwave at room temperature. Band gaps were estimated experimentally by UV-Vis diffuse reflectance spectroscopy, and theoretically using the first-principle calculations, as described in Supplementary Information 1.2. The photocatalytic activity of samples was examined by measuring the degradation rate of Rhodamine B (RhB) under UV and visible light (see Supplementary Information 1.3 for details), and the active surface area of photocatalytic samples was measured using the Brunauer-Emmett-Teller (BET) and pulsed nuclear magnetic resonance (NMR) methods (see Supplementary Information 1.4 for details).

Results and Discussion

XRD results, by CuKα radiation, are shown in Fig. 1(c) for wurtzite powder and samples processed by HPT under 3 and 6 GPa. Wurtzite peaks are clearly visible in the powder and in the HPT-processed samples, with a distinct peak broadening after HPT processing due to the lattice strain effect and formation of nanograins with an average size of 11 ± 5 nm (see high-resolution TEM micrographs in Supplementary Figs. 1 and 2). In addition to wurtzite, the rocksalt phase with a fraction of 50 wt.% can be detected for the sample processed by HPT under 6 GPa. The presence of rocksalt phase, which remained stable at least for 220 days at ambient condition, confirms that simultaneous introduction of pressure and strain is essential for stabilizing the rocksalt phase at ambient pressure. Unlike oxides like $BaTiO_3$,[31] Y_2O_3[37] and TiO_2[39] in which high-pressure phases remain stable in grains with sizes smaller than a critical size, a correlation between grain size and crystal structure could not be confirmed for ZnO because of the less stable feature of rocksalt phase when irradiated by electron beam during the TEM examinations.

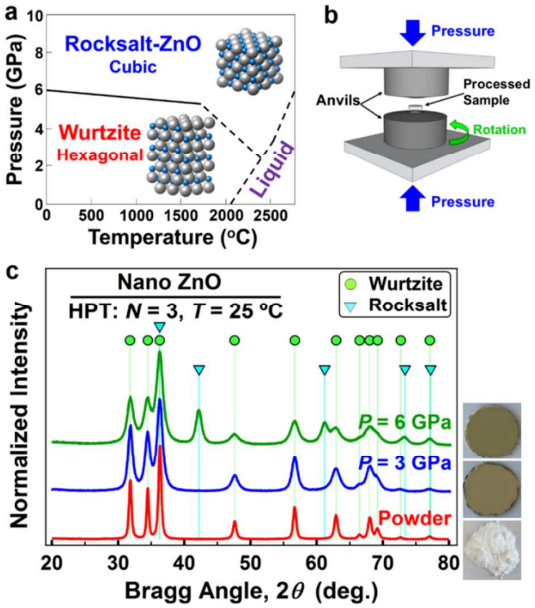

Fig. 1 (a) Phase diagram of ZnO, (b) Schematic illustration of HPT, and (c) XRD results by CuKα radiation before/after HPT including images of samples.

Another feature that can be seen in Fig. 1(c) is that the colour of samples changes from white to yellow after HPT processing due to the formation of point defects such as oxygen vacancies[40-42]. Formation of oxygen vacancies as point defects after HPT processing is also evident from the synchrotron XRD peak shifts (see Supplementary Fig. 3 in which peaks corresponding to 002 and 101 planes shift to lower angles). Raman spectra in Fig. 2a also show that in addition to the vibration modes related to the wutrzite phase, a peak at 577 cm^{-1} appears after HPT processing, indicative of oxygen vacancies.[16, 43, 44] It is noted that the rocksalt phase has no Raman active modes[28]. A broad PL emission at 587 nm (orange emission in Supplementary Fig. 4) is also observed in HPT-processed samples probably due to the radiative recombination of photo-excited holes and singly ionized oxygen vacancies in ZnO samples.[45] Some other emission colours such as yellow[46], green[41, 47] and blue[48, 49] have been reported for different defect states in ZnO, although the origin of these emissions is not well understood.[50] EPR is another effective method for investigating paramagnetic oxygen vacancy defects. EPR signals in Fig. 2b show that two major g values of 1.960 and 1.997 exist for the HPT-processed samples, both of which are absent in the ZnO powder. Although there is a big argument over the origin of g = 1.960 whether it is due to the oxygen vacancies,[47] shallow donors,[51] electrons in the conduction band,[52] or electrons in the donor band,[52] it is widely accepted that g = 1.997 is due to oxygen vacancies.[50, 53] The presence of oxygen vacancies after HPT processing, which is also reported in $BaTiO_3$[34]

and TiO_2,[38] is due to the effect of strain on continuous formation of vacancies, and the effect of high pressure on suppressing the migration and annihilation of the vacancies.[54]

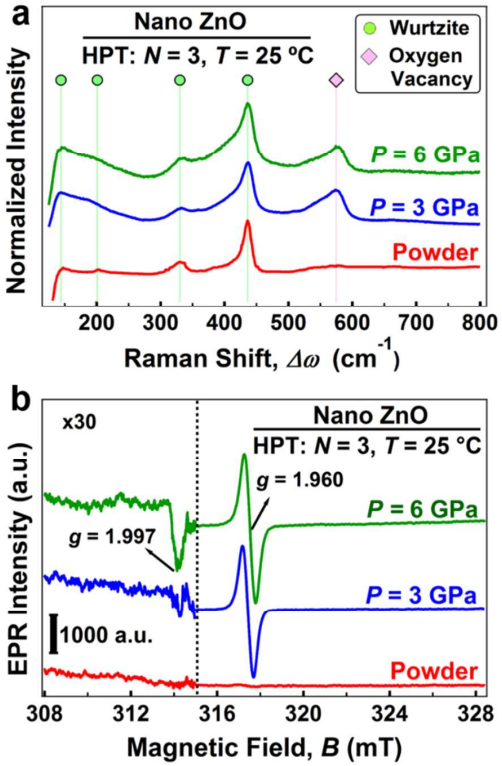

Fig. 2 (a) Raman spectra and (b) EPR spectra of ZnO before/after HPT processing.

Fig. 3a shows the UV-Vis diffused reflectance spectra of the starting powder (wurtzite without oxygen vacancies), the sample processed by HPT under 3 GPa (wurtzite with oxygen vacancies) and the sample processed by HPT under 6 GPa (rocksalt with oxygen vacancies). All samples show an intense absorption below the absorption-edge wavelength. The absorption edge of initial powder is at ~400 nm, while it redshifts to the visible light region with absorption edge of about 460 and 650 nm for the samples processed by HPT under 3 and 6 GPa, respectively. An appreciable tail absorbance is also observed for the HPT-processed samples because of the presence of oxygen vacancies, which can form localized states in the band gap.[55] Band gap of samples are estimated from the UV-Vis diffused reflectance spectra based on the Kubelka-Munk theory.[56] As shown in Fig. 3b, the estimated band gaps are 3.1, 2.8, and 1.8 eV for the starting powder and for the samples processed by HPT under 3 and 6 GPa, respectively. The estimated band gap for the starting powder is well consistent with the reported band gap for the wurtzite ZnO in the literature (3.1-3.4 eV).[4, 8] A decrease in the band gap of sample processed at 3 GPa is also consistent with previous reports, where the band gap of ZnO decreases with introduction of oxygen vacancies.[16, 57, 58] Oxygen vacancies create energy states above the valance band and leads to reducing the band gap by lifting the position of valance band. However, the significant band gap narrowing of sample processed under 6 GPa cannot be explained solely by the presence of oxygen vacancies but it is a consequence of rocksalt-phase formation. A list of representative published data gathered in Supplementary Table 1 reveals that the band gap of 1.8 eV obtained in this work is the narrowest among the reported values for pure ZnO.

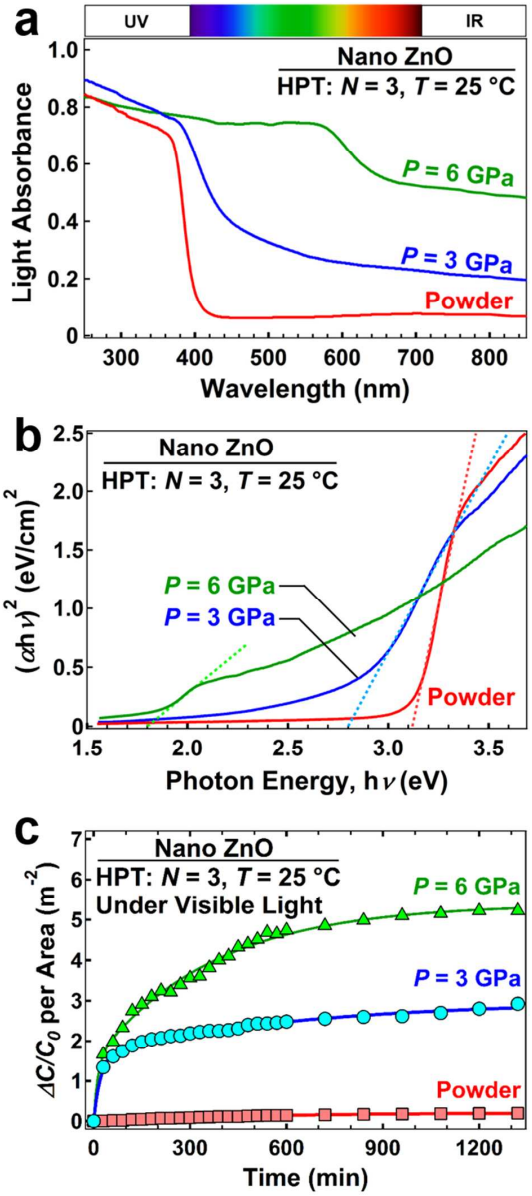

Fig. 3 (a) UV-Vis diffused reflectance spectra, (b) bandgap estimation based on Kubelka-Munk theory, and (c) photocatalytic activity for RhB degradation under visible light for ZnO before/after HPT processing (ΔC: degraded amount of RhB, C_0: initial conce

Photocatalytic activity of samples under visible light is shown in Fig. 3c (see Supplementary Fig. 5 for the results under UV light). It should be noted that the data in Fig. 3c were normalized by surface area of each sample measured by pulsed NMR because a significant powder consolidation occurs during HPT processing of oxides (see Supplementary Fig. 6 and Table 2).[59] While wurtzite powder shows minor RhB photodegradation under visible light, the sample processed by HPT under 3 GPa exhibits higher photocatalytic activity due to the formation of oxygen vacancies.[16, 60, 61] The sample processed at 6 GPa shows superior activity than others due to the rocksalt-phase formation with a band gap of 1.8 eV, which can absorb more visible light. It is noteworthy that, on one hand the rocksalt phase is quite stable in water solution and after photocatalytic activity test (see Supplementary Fig. 7), but on the other hand it is unstable when it is irradiated to high energy light sources such as X-ray and electron beam (see Supplementary Figs. 8 and 9).

The calculated density of states (DOS) for zinc and oxygen atoms together with the total density of states are shown in Fig. 4 for (a) wurtzite without lattice defects, (b) wurtzite with 6.25 at.% of oxygen vacancies, (c) rocksalt without lattice defects, and (d) rocksalt with 6.25 at.% of oxygen vacancies. Corresponding supercells and calculated band gaps of each sample are also shown in Fig. 4 (details of calculation results are summarized in Supplementary Table 3). The band gap of ideal wurtzite is calculated as 3.22 eV, which is in good agreement with the experimentally measured value in this study, 3.1 eV. Introduction of oxygen vacancy to wurtzite reduces its band gap to 2.91 eV, which is well consistent with the presented results in Fig. 3b. The calculated band gap of defect-free rocksalt phase is 3.25 eV, but it significantly reduces to 1.73 eV with introduction of oxygen vacancies in good agreement with the experimental results in Fig. 3b. Despite earlier theoretical studies which estimated a low band gap for the rocksalt phase in the range of 1.2-2.6 eV[24-26], the current calculation and experimental results suggest that the oxygen vacancies should be present in the high-pressure rocksalt phase to achieve a low band gap and develop superior visible-light photocatalytic activity.

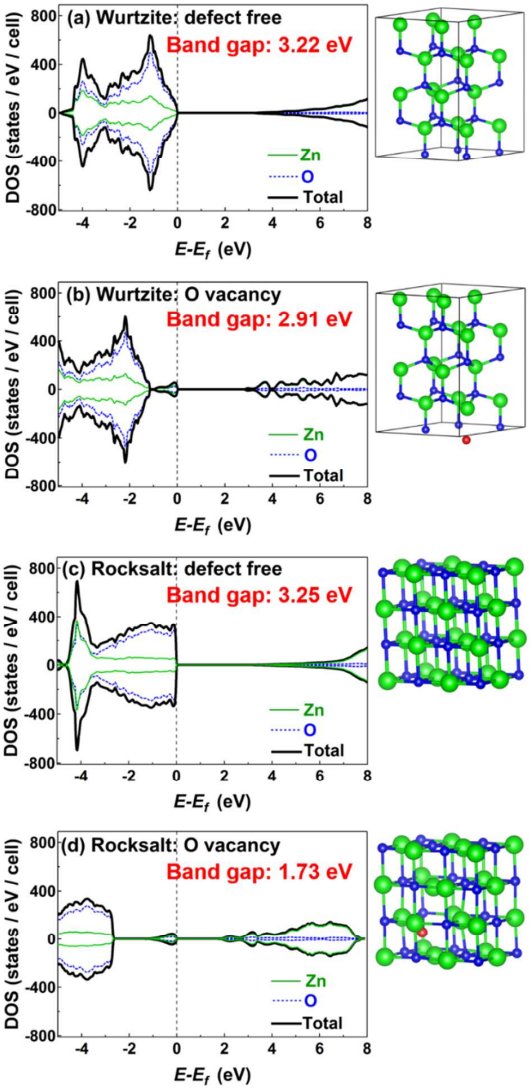

Fig. 4 DOS profiles calculated by first-principles calculations with corresponding supercells and band gap values for (a) ideal wurtzite, (b) wurtzite with 6.25% of oxygen vacancies, (c) ideal rocksalt, and (d) rocksalt with 6.25% of oxygen vacancies (*E*: Energy; E_f: Fermi level).

Conclusions

High-pressure rocksalt ZnO phase with large fraction of oxygen vacancies was stabilized at ambient pressure by torsional straining under 6 GPa. The stabilized rocksalt phase exhibited a low band gap of 1.8 eV in good agreement with the first-principles calculations. The material exhibited superior photocatalytic activity under visible light to photodegrade the RhB dye.

Acknowledgements

KE thanks Kyushu University for the Qdai-Jump Research grant (No. 28325) and the MEXT, Japan, for a Grant-in-Aid for Scientific Research (B) (No. 16H04539). JW thanks a funding from JSPS and NSF, Japan, under the JSPS-NSF Partnership for International Research and Education (PIRE). This study was supported in part by Japan Science and Technology Adaptable and Seamless Technology transfer Program through target-driven R&D (JST A-STEP), Japan, in part by Core Research for Evolutional Science and Technology (CREST), in part by a Grant-in-Aid for Scientific Research (S) from the MEXT, Japan (No. 26220909), and in part by WPI-I^{2}CNER. The HPT process was carried out in the International Research Centre on Giant Straining for Advanced Materials (IRC-GSAM) at Kyushu University.

References

1. B. O'Regan and M. Gratzel, *Nature*, 1991, **353**, 737-740.
2. R. Asahi, T. Morikawa, T. Ohwaki, K. Aoki and Y. Taga, *Science*, 2001, **293**, 269-271.
3. M. R. Hoffmann, S. T. Martin, W. Choi and D. W. Bahnemann, *Chem. Rev.*, 1995, **95**, 69-96.
4. Z. L. Wang, *ACS Nano*, 2008, **2**, 1987-1992.
5. P. Patra, S. Mitra, N. Debnath and A. Goswami, *Langmuir*, 2012, **28**, 16966-16978.
6. W. Zhong Lin, *J. Phys. Condens. Matter.*, 2004, **16**, R829.
7. D. Liu and T. L. Kelly, *Nat. Photon.*, 2014, **8**, 133-138.
8. V. Srikant and D. R. Clarke, *J. Appl. Phys.*, 1998, **83**, 5447-5451.
9. M. Romero, J. Blanco, B. Sánchez, A. Vidal, M. Sixto, A. I. Cardona and E. Garcia, *Sol. Energy*, 1999, **66**, 169-182.
10. J. Nowotny, C. C. Sorrell, L. R. Sheppard and T. Bak, *Int. J. Hydrogen Energy*, 2005, **30**, 521-544.
11. D. Chen, H. Zhang, S. Hu and J. Li, *J. Phys. Chem. C*, 2008, **112**, 117-122.
12. Z. Zhang, C. Shao, X. Li, L. Zhang, H. Xue, C. Wang and Y. Liu, *J. Phys. Chem. C*, 2010, **114**, 7920-7925.
13. L.-C. Jiang, W.-D. Zhang, Y.-X. Yu and J. Wang, *Electrochem. Commun.*, 2011, **13**, 627-630.
14. H. Fu, T. Xu, S. Zhu and Y. Zhu, *Environ. Sci. Technol.*, 2008, **42**, 8064-8069.
15. F. Kayaci, S. Vempati, I. Donmez, N. Biyikli and T. Uyar, *Nanoscale*, 2014, **6**, 10224-10234.
16. J. Wang, Z. Wang, B. Huang, Y. Ma, Y. Liu, X. Qin, X. Zhang and Y. Dai, *ACS Appl. Mater. Interfaces*, 2012, **4**, 4024-4030.
17. X. Qiu, L. Li, J. Zheng, J. Liu, X. Sun and G. Li, *J. Phys. Chem. C*, 2008, **112**, 12242-12248.
18. Y.-Z. Zheng, X. Tao, Q. Hou, D.-T. Wang, W.-L. Zhou and J.-F. Chen, *Chem. Mater.*, 2011, **23**, 3-5.
19. S. Anandan, A. Vinu, T. Mori, N. Gokulakrishnan, P. Srinivasu, V. Murugesan and K. Ariga, *Catal. Commun.*, 2007, **8**, 1377-1382.
20. S. G. Kumar and K. S. R. K. Rao, *RSC Adv.*, 2015, **5**, 3306-3351.
21. J. Tao, T. Luttrell and M. Batzill, *Nat. Chem.*, 2011, **3**, 296-300.
22. X. Chen, L. Liu, P. Y. Yu and S. S. Mao, *Science*, 2011, **331**, 746-750.
23. S. Wendt, P. T. Sprunger, E. Lira, G. K. H. Madsen, Z. Li, J. Ø. Hansen, J. Matthiesen, A. Blekinge-Rasmussen, E. Lægsgaard, B. Hammer and F. Besenbacher, *Science*, 2008, **320**, 1755-1759.
24. A. Segura, J. A. Sans, F. J. Manjón, A. Muñoz and M. J. Herrera-Cabrera, *Appl. Phys. Lett.* , 2003, **83**, 278-280.
25. A. Alvarado, J. Attapattu, Y. Zhang and C. Chen, *J. Appl. Phys.*, 2015, **118**, 165101.
26. H. Dixit, R. Saniz, D. Lamoen and B. Partoens, *J. Phys. Condens. Matter.*, 2010, **22**, 125505.
27. F. Decremps, J. Pellicer-Porres, A. M. Saitta, J.-C. Chervin and A. Polian, *Phys. Rev. B*, 2002, **65**, 092101.
28. J. Pellicer-Porres, A. Segura, V. Panchal, A. Polian, F. Decremps and P. Dumas, *Phys. Rev. B*, 2011, **84**, 125202.
29. L. Bayarjargal and B. Winkler, *Appl. Phys. Lett.* , 2012, **100**, 021909.
30. P. W. Bridgman, *Phys. Rev.*, 1935, **48**, 825-847.
31. R. Z. Valiev, Y. Estrin, Z. Horita, T. G. Langdon, M. J. Zechetbauer and Y. T. Zhu, *JOM*, 2006, **58**, 33-39.
32. K. Edalati, T. Daio, Y. Ikoma, M. Arita and Z. Horita, *Appl. Phys. Lett.* , 2013, **103**, 034108.
33. K. Edalati, T. Daio, M. Arita, S. Lee, Z. Horita, A. Togo and I. Tanaka, *Acta Mater.*, 2014, **68**, 207-213.
34. K. Edalati, M. Arimura, Y. Ikoma, T. Daio, M. Miyata, D. J. Smith and Z. Horita, *Mater. Res. Lett.* , 2015, **3**, 216-221.
35. V. I. Levitas and M. Javanbakht, *Nanoscale*, 2014, **6**, 162-166.
36. K. Edalati, T. Daio, Y. Ikoma, M. Arita and Z. Horita, *Appl. Phys. Lett.*, 2013, **103**, 034108.
37. H. Razavi-Khosroshahi, K. Edalati, H. Emami, E. Akiba, Z. Horita and M. Fuji, *Inorg. Chem.*, 2017, DOI: 10.1021/acs.inorgchem.6b02725.
38. H. Razavi-Khosroshahi, K. Edalati, M. Hirayama, H. Emami, M. Arita, M. Yamauchi, H. Hagiwara, S. Ida, T. Ishihara, E. Akiba, Z. Horita and M. Fuji, *ACS Catal.*, 2016, **6**, 5103-5107.
39. H. Razavi-Khosroshahi, K. Edalati, M. Arita, Z. Horita and M. Fuji, *Scripta Mater.*, 2016, **124**, 59-62.
40. S. R. Lingampalli, K. Manjunath, S. Shenoy, U. V. Waghmare and C. N. R. Rao, *J. Am. Chem. Soc.*, 2016, **138**, 8228-8234.
41. S. G. Ullattil, P. Periyat, B. Naufal and M. A. Lazar, *Ind. Eng. Chem. Res.*, 2016, **55**, 6413-6421.
42. N. Y. Garces, N. C. Giles, L. E. Halliburton, G. Cantwell, D. B. Eason, D. C. Reynolds and D. C. Look, *Appl. Phys. Lett.* , 2002, **80**, 1334
43. X. Xue, T. Wang, X. Jiang, J. Jiang, C. Pan and Y. Wu, *CrystEngComm*, 2014, **16**, 1207-1216.
44. D. Chen, Z. Wang, T. Ren, H. Ding, W. Yao, R. Zong and Y. Zhu, *J. Phys. Chem. C*, 2014, **118**, 15300-15307.
45. A. B. Djurišić, W. C. H. Choy, V. A. L. Roy, Y. H. Leung, C. Y. Kwong, K. W. Cheah, T. K. Gundu Rao, W. K. Chan, H. Fei Lui and C. Surya, *Adv. Funct. Mater.*, 2004, **14**, 856-864.
46. X. L. Wu, G. G. Siu, C. L. Fu and H. C. Ong, *Appl. Phys. Lett.*, 2001, **78**, 2285-2287.
47. K. Vanheusden, C. H. Seager, W. L. Warren, D. R. Tallant and J. A. Voigt, *Appl. Phys. Lett.*, 1996, **68**, 403-405.
48. L. Dai, X. L. Chen, W. J. Wang, T. Zhou and B. Q. Hu, *J. Phys. Condens. Matter.*, 2003, **15**, 2221.
49. Z. Y. Xue, D. H. Zhang, Q. P. Wang and J. H. Wang, *Appl. Surf. Sci.*, 2002, **195**, 126-129.
50. A. Janotti and C. G. Van de Walle, *Phys. Rev. B*, 2007, **76**, 165202.
51. N. Y. Garces, L. Wang, L. Bai, N. C. Giles, L. E. Halliburton and G. Cantwell, *Appl. Phys. Lett.*, 2002, **81**, 622-624.
52. N. Y. Garces, N. C. Giles, L. E. Halliburton, G. Cantwell, D. B. Eason, D. C. Reynolds and D. C. Look, *Appl. Phys. Lett.*, 2002, **80**, 1334-1336.
53. L. S. Vlasenko and G. D. Watkins, *Phys. Rev. B*, 2005, **71**, 125210.
54. B. Oberdorfer, B. Lorenzoni, K. Unger, W. Sprengel, M. Zehetbauer, R. Pippan and R. Würschum, *Scripta Mater.*, 2010, **63**, 452-455.
55. P. Nagpal and V. I. Klimov, *Nat. Commun.*, 2011, **2**, 486.
56. J. I. Pankove, *Optical Processes in Semiconductors*, Dover Publications, New York, 1971.
57. H. Liu, F. Zeng, Y. Lin, G. Wang and F. Pan, *Appl. Phys. Lett.*, 2013, **102**, 181908.

58. A. Asok, M. N. Gandhi and A. R. Kulkarni, *Nanoscale*, 2012, **4**, 4943-4946.
59. K. Edalati and Z. Horita, *Scripta Mater.*, 2010, **63**, 174-177.
60. A. S. French, A. A. Sokol, S. T. Bromley, C. R. A. Catlow, S. C. Rogers, F. King and P. Sherwood, *Angew. Chem. Int. Ed.*, 2001, **40**, 4437–4440.
61. M. Kurtz, J. Strunk, O. Hinrichsen, M. Muhler, K. Fink, B. Meyer and C. Wöll, *Angew. Chem. Int. Ed.*, 2005, **44**, 2790-2794.